

Theoretical study of pulse delay effects in the photoelectron angular distribution of near-threshold EUV+IR two-photon ionization of atoms

Kenichi L. Ishikawa*

*Department of Nuclear Engineering and Management, Graduate School of Engineering,
The University of Tokyo, 7-3-1 Hongo, Bunkyo-ku, Tokyo 113-8656, Japan and
Photon Science Center, Graduate School of Engineering,
The University of Tokyo, 7-3-1 Hongo, Bunkyo-ku, Tokyo 113-8656, Japan*

A. K. Kazansky

*Departamento de Fisica de Materiales, UPV/EHU, E-20018 San Sebastian/Donostia, Spain
Donostia International Physics Center (DIPC), E-20018 San Sebastian/Donostia, Spain and
IKERBASQUE, Basque Foundation for Science, E-48011 Bilbao, Spain*

N. M. Kabachnik

*Skobeltsyn Institute of Nuclear Physics, Lomonosov Moscow State University, Moscow 119991, Russia and
European XFEL, D-22761 Hamburg, Germany*

Kiyoshi Ueda

*Institute of Multidisciplinary Research for Advanced Materials,
Tohoku University, Katahira 2-1-1, Aoba-ku, Sendai 980-8577, Japan*

(Dated: June 21, 2021)

We theoretically study the photoelectron angular distributions (PADs) from two-color two-photon near-threshold ionization of hydrogen and noble gas (He, Ne, and Ar) atoms by a combined action of femtosecond extreme ultraviolet (EUV) and near-infrared (IR) laser pulses. Using the second-order time-dependent perturbation theory, we clarify how the two-photon ionization process depends on EUV-IR pulse delay and how it is connected to the interplay between resonant and nonresonant ionization paths. Furthermore, by solving the time-dependent Schrödinger equation, we calculate the anisotropy parameters β_2 and β_4 as well as the amplitude ratio and relative phase between partial waves characterizing the PADs. We show that in general these parameters notably depend on the time delay between the EUV and IR pulses, except for He. This dependence is related to the varying relative role of resonant and nonresonant paths of photoionization. Our numerical results for H, He, Ne, and Ar show that the pulse-delay effect is more pronounced for p -shell ionization than for s -shell ionization.

PACS numbers: 32.80.Rm, 32.80.Fb, 41.60.Cr, 42.65.Ky

I. INTRODUCTION

Investigations of non-linear (multiphoton) processes in extreme ultraviolet (EUV) and soft x-ray energy range is a quickly developing branch of photon-matter interaction studies. It has been strongly stimulated by the construction and operation of EUV and x-ray free electron lasers (FELs) as well as by the progress in powerful laser physics which results in creation of photon sources based on high-harmonic generation. Intense ultra-short photon pulses from FEL allows one to investigate the non-linear EUV processes using well developed methods of photoelectron spectroscopy including measurements of photoelectron angular distributions (PADs), which proved to be a sensitive tool for studying the dynamics of photoprocesses [1].

One of the most basic non-linear processes is a two-photon single ionization (TPSI) of atoms where an atomic electron is emitted by a simultaneous absorption of two photons. The TPSI (and multi photon ionization more generally) has been

intensively investigated theoretically for decades (see e.g.[2–17]) as well as experimentally since the advent of high-harmonic sources and FELs [18–24]. Both the absolute cross section of TPSI [25] and the angular distribution of photoelectrons [26] have been recently measured for He.

One of the fundamental problems of TPSI is a relative contribution of resonant and non-resonant (direct) ionization mechanisms. Absorption of two photons involves intermediate states of the system. In general, according to the rules of quantum mechanics, one should take into account contributions of all excited intermediate states, both discrete and continuous. In the resonance-enhanced case, i.e., if the photon energy spectrum allows resonant excitation of one or more excited states, the resonant ionization process via resonant levels and the nonresonant process via nonresonant intermediate levels coexist [3, 27, 28]. For a sufficiently long pulse resonant with an excited level, the contribution from the resonant process is dominant, and the TPSI cross section can be calculated within the two-step approach: excitation of the resonant state and its subsequent ionization. If we use an ultrashort (femtosecond) exciting pulse with a large bandwidth, on the other hand, the co-presence of resonant and nonresonant contributions becomes a more complex problem.

*Electronic address: ishiken@n.t.u-tokyo.ac.jp

It has recently been theoretically demonstrated [27, 28] that the angular distribution of photoelectrons in TPSI generated by ultrashort EUV pulses changes with the pulse width, reflecting the competition between resonant and nonresonant ionization paths. Calculations for H and He atoms have shown that the relative phase δ between S and D ionization channels is distinct from the scattering phase shift difference and varies with the pulse width and that this variation is different for different photon energies. This prediction has been confirmed experimentally [26] for the case of He.

The above discussion, which originally concerns single-color TPSI, is quite general and can also be extended to two-color cases. Specifically let us consider a combined action of an EUV pulse from FEL or high-harmonic source and of a synchronized optical laser pulse. Such two-color multiphoton ionization experiments have proved to be useful for characterization of ultrashort EUV pulses as well as for a detailed investigation of ionization dynamics [29–33] (see also review [34]). Here also the measurements of PADs provided deeper insight into the physics of the photon-atom interaction [35–42]. One of the advantages of the two-color investigation is that the two pulses can be independently controlled; one has possibility to vary the frequency, duration and polarization of the EUV and optical pulses independently. This gives much more flexibility to the experiment. One additional advantage is that in two-color experiments with ultrashort pulses one can study the time-evolution of the ionization process by controlling the time delay between them.

Recently this additional degree of freedom has been used to advantage in Ref. [43]. It was shown experimentally that the PAD in two-color TPSI of Ne atoms is notably different for temporally overlapping and non-overlapping EUV and IR pulses. The difference between these two extreme cases clearly demonstrates that the PAD in TPSI strongly depends on the time delay between the pulses. The corresponding theoretical calculations agree with the measurements and explain the dependence by the change in the relative contribution of resonant and nonresonant ionization paths[43].

In the present work we extend our previous works [26–28, 43] and theoretically investigate in more detail the pulse-delay dependence of photoelectron energy spectra and angular distributions, both energy-resolved and integrated, in near-threshold two-color TPSI, with focus on resonant and nonresonant contributions. We first describe two-color TPSI with the second-order time-dependent perturbation theory and show how the interplay between the resonant and nonresonant paths depends on the pulse delay. Then, we study the pulse-delay effect for different target atoms (H, He, Ne, and Ar), based on direct numerical simulation of the time-dependent Schrödinger equation (TDSE).

This paper is organized as follows. In the next section, us-

ing the perturbation theory, we discuss the general idea of the relation between the pulse-delay dependence of the final-state amplitude for two-color TPSI and the contribution of resonant and nonresonant ionization paths. We then shortly describe the numerical methods used to solve TDSE and calculate anisotropy parameters. In Sec. IV we present and discuss the simulation results for H, He, Ne and Ar atoms. Our conclusions and outlook are presented in Sec. V.

II. ANALYSIS BASED ON THE PERTURBATION THEORY

To illustrate the main idea it is instructive to consider the problem of TPSI within the second-order time-dependent perturbation theory. Generalizing the expression for the amplitude of the two-photon transition presented in Ref. [44] to the case of multiple intermediate levels, we can write the amplitude of the final state f of the atom as (atomic units are used throughout unless otherwise indicated)

$$c_f = i \sum_{\alpha} \mu_{f\alpha} \mu_{\alpha i} \left[i\pi \hat{E}(\omega_{\alpha i}) \hat{E}(\omega_{f\alpha}) + P \int_{-\infty}^{\infty} \frac{\hat{E}(\omega) \hat{E}(\omega_{fi} - \omega)}{\omega_{\alpha i} - \omega} d\omega \right], \quad (1)$$

where $\mu_{\alpha i}$ etc. denote the dipole transition matrix element between state i and α ; i is the initial state, α the intermediate states (α should be taken as a collection of quantum numbers that specify each energy eigenstate, e.g., $\alpha = (n, l, m)$ for bound states and $\alpha = (\epsilon, l, m)$ for continuum states for the case of a hydrogen-like atom); $\omega_{\alpha i} = \omega_{\alpha} - \omega_i$ etc., P is the Cauchy principal value, and $\hat{E}(\omega)$ the Fourier transform of the electric field $E(t)$ of the ionizing pulse. In principle, the sum should be taken over all the bound and continuum intermediate states α . The first and second terms of Eq. (1) can be interpreted as the resonant (or two-step) and non-resonant processes, respectively.

Let us consider a double (EUV + IR) pulse of the form:

$$E(t) = E_X(t) + E_{IR}(t - \tau), \quad (2)$$

and its Fourier transform:

$$\hat{E}(\omega) = \hat{E}_X(\omega) + \hat{E}_{IR}(\omega) e^{i\omega\tau}, \quad (3)$$

where the first and the second terms correspond to the EUV and IR pulses, respectively, and τ denotes the delay between the pulses. In this case, neglecting resonant excitation from the ground state by an IR photon [i.e., $\hat{E}_{IR}(\omega_{\alpha i}) \approx 0$ for any α], Eq. (1) can be approximated by

$$c_f = i \sum_{\alpha} \mu_{f\alpha} \mu_{\alpha i} \left[i\pi \hat{E}_X(\omega_{\alpha i}) \hat{E}_{IR}(\omega_{f\alpha}) e^{i\omega_{f\alpha}\tau} + P \int_{-\infty}^{\infty} \frac{\hat{E}_X(\omega_{f_i} - \omega) \hat{E}_{IR}(\omega) e^{i\omega\tau} + \hat{E}_X(\omega) \hat{E}_{IR}(\omega_{f_i} - \omega) e^{i(\omega_{f_i} - \omega)\tau}}{\omega_{\alpha i} - \omega} d\omega \right] \quad (4)$$

$$= i \sum_{\alpha} \mu_{f\alpha} \mu_{\alpha i} \left[i\pi \hat{E}_X(\omega_{\alpha i}) \hat{E}_{IR}(\omega_{f\alpha}) e^{i\omega_{f\alpha}\tau} + P \int_{-\infty}^{\infty} \hat{E}_X(\omega_{f_i} - \omega) \hat{E}_{IR}(\omega) e^{i\omega\tau} \left(\frac{1}{\omega_{\alpha i} - \omega} - \frac{1}{\omega_{f\alpha} - \omega} \right) d\omega \right]. \quad (5)$$

When the two pulses overlap ($\tau = 0$),

$$c_f = i \sum_{\alpha} \mu_{f\alpha} \mu_{\alpha i} \left[i\pi \hat{E}_X(\omega_{\alpha i}) \hat{E}_{IR}(\omega_{f\alpha}) + P \int_{-\infty}^{\infty} \hat{E}_X(\omega_{f_i} - \omega) \hat{E}_{IR}(\omega) \left(\frac{1}{\omega_{\alpha i} - \omega} - \frac{1}{\omega_{f\alpha} - \omega} \right) d\omega \right], \quad (6)$$

thus, both the first (resonant) and second (non-resonant) terms contribute to c_f , leading to an additional phase and to a photoelectron angular distribution (PAD) different from the one expected from the scattering phase shifts. With increasing delay, factors $e^{i\omega_{f\alpha}\tau}$ and $e^{i\omega\tau}$ begin to oscillate, and the PAD changes with τ .

For large delay, Eq. (5) can be transformed, after some algebra, into

$$c_f = -\pi \times \sum_{\alpha} \mu_{f\alpha} \mu_{\alpha i} [1 + \text{sgn}(\tau)] \hat{E}_{IR}(\omega_{f\alpha}) \hat{E}_X(\omega_{\alpha i}) e^{i\omega_{f\alpha}\tau}, \quad (7)$$

where we have used the relation

$$P \int_{-\infty}^{\infty} \frac{e^{i\omega\tau}}{\omega_0 - \omega} d\omega = -i\pi e^{i\omega_0\tau} \text{sgn}(\tau). \quad (8)$$

If the EUV spectrum is located within the Rydberg manifold, a Rydberg wave packet is formed by the EUV pulse and then ionized by the IR pulse. The factor $e^{i\omega_{f\alpha}\tau}$ describes the evolution of the Rydberg wave packet with increasing delay τ . The ionization yield $|c_f|^2$ changes with τ , reflecting the Kepler-like motion of the Rydberg wave packet, while the PAD only slightly changes (nearly constant) with τ . There is no ionization ($c_f = 0$) if the IR pulse precedes the EUV pulse ($\tau < 0$), as is evident if one considers in the time domain. Apparently, Eq. (7) indicates that there are only resonant paths, which might sound obvious again in the time-domain consideration. It should be, however, noticed that the second term in the sum in Eq. (7) originates from the second term in Eq. (6), usually interpreted as non-resonant paths. This observation implies that the attribution of resonant and non-resonant processes may be somewhat arbitrary.

In the above-threshold case, where the EUV spectrum lies above the ionization threshold, the two-photon ionization yield vanishes if the two-pulses are separated in time. This intuitively obvious result can be shown as follows. Assuming that the transition matrix elements in Eq. (7) are almost constant within the bandwidth of the pulses, one finds,

$$c_f \propto \int_{-\infty}^{\infty} \hat{E}_{IR}(\omega_{f\alpha}) \hat{E}_X(\omega_{\alpha i}) e^{i\omega_{f\alpha}\tau} d\omega_{\alpha}. \quad (9)$$

After some algebra using Parseval's theorem:

$$\int_{-\infty}^{\infty} \hat{f}(\omega) \hat{g}(\omega) d\omega = \int_{-\infty}^{\infty} f(t) g(-t) dt, \quad (10)$$

one obtains,

$$\int_{-\infty}^{\infty} \hat{E}_{IR}(\omega_{f\alpha}) \hat{E}_X(\omega_{\alpha i}) e^{i\omega_{f\alpha}\tau} d\omega_{\alpha} = \int_{-\infty}^{\infty} E_X(t) E_{IR}(t - \tau) e^{-i\omega_{f\alpha}\tau} dt, \quad (11)$$

which vanishes if the XUV and IR pulses do not overlap each other at all, i.e., $E_X(t) E_{IR}(t - \tau) = 0$ for any t .

III. NUMERICAL SOLUTION OF TIME-DEPENDENT SCHRÖDINGER EQUATION

In the numerical calculations discussed below, we consider the case where the EUV photon energy is slightly below the ionization threshold. We have chosen the following basic parameters of the pulses which are rather common in recent experiments: the IR pulse with the carrier frequency $\omega_L = 1.55$ eV (800 nm) has a duration of 30 fs (FWHM of intensity). The peak intensity of the IR field is 10^{10} W/cm² which is sufficiently low to guarantee that only one IR photon is absorbed in ionization. The duration of the EUV pulse is 8 fs (FWHM of intensity), typical of a coherent time of an EUV FEL pulse [24]. The time delay between maxima of the pulses is varied from 0 (complete overlap of the pulses) to 160 fs at most. The EUV photon energy $\hbar\omega_X$ is chosen to be by 0.2 eV smaller than the ionization potential I_p of each atom, i.e., the excess energy $E_{ex} \equiv \hbar\omega_X - I_p$ is -0.2 eV.

We assume that both the EUV and IR pulses are linearly polarized along the z direction. The photoelectron angular distribution from two-photon ionization is given by [45],

$$I(\theta) = \frac{\sigma}{4\pi} [1 + \beta_2 P_2(\cos \theta) + \beta_4 P_4(\cos \theta)], \quad (12)$$

where σ is the total cross section, θ is the angle between the laser polarization and the electron velocity vector, and β_2 and

β_4 are the anisotropy parameters associated with the second- and fourth-order Legendre polynomials, $P_2(x)$ and $P_4(x)$, respectively.

Although in principle it would be possible to calculate PADs using the analytical expression given in the previous section, it would be very complicated to perform an integration over all the bound and continuum intermediate states.

$$i \frac{\partial \Phi(\mathbf{r}_1, \dots, \mathbf{r}_n, t)}{\partial t} = \left[\hat{H}_e(\mathbf{r}_1, \dots, \mathbf{r}_n) - \sum_i^n z_i (E_X(t) + E_{IR}(t - \tau)) \right] \Phi(\mathbf{r}_1, \dots, \mathbf{r}_n, t), \quad (13)$$

where $\Phi(\mathbf{r}_1, \dots, \mathbf{r}_n, t)$ denotes the wave function of the atom and $\hat{H}_e(\mathbf{r}_1, \dots, \mathbf{r}_n)$ the field-free atomic Hamiltonian.

We exactly solve the TDSE (13) for H and He, while we make some additional approximations for the case of multi-electron atoms (Ne and Ar). Below we briefly summarize the numerical methods applied in this paper.

A. Hydrogen atom

For a hydrogen atom the TDSE (13) is reduced to,

$$i \frac{\partial \Phi(\mathbf{r}, t)}{\partial t} = \left[-\frac{1}{2} \nabla^2 - \frac{1}{r} - z(E_X(t) + E_{IR}(t - \tau)) \right] \Phi(\mathbf{r}, t). \quad (14)$$

Equation (14) is numerically integrated using the alternating direction implicit (Peaceman-Rachford) method [13, 17, 46–53]. Sufficiently long (typically a few times the pulse width) after the pulse has ended, the ionized wave packet moving outward in time is spatially well separated and clearly distinguishable from the non-ionized part remaining around the origin. We calculate the parameters β_2 and β_4 by integrating the ionized part of $|\Phi(\mathbf{r})|^2$ over r and ϕ .

For the case of s-shell ionization (H and He) by two dipole photons, the angular distribution of photoelectrons is determined by the interference of the S and D wave packets [27, 28],

$$I(\theta) \propto |\tilde{c}_S e^{i\delta_0} Y_{00} - \tilde{c}_D e^{i\delta_2} Y_{20}|^2, \quad (15)$$

where Y_{00} and Y_{20} are spherical functions, \tilde{c}_S and \tilde{c}_D are real numbers that have the same absolute values as complex amplitudes c_S and c_D , respectively, and δ_l the phase of the partial wave, or the *apparent* phase shift. The apparent phase shift difference,

$$\delta \equiv \delta_0 - \delta_2 = \delta_{sc} + \delta_{ex}, \quad (16)$$

consists of a part δ_{sc} intrinsic to the continuum eigenfunctions (scattering phase shift difference), which has previously been

studied both theoretically [54–56] and experimentally [38], and the extra contribution $\delta_{ex} = \arg c_S/c_D$ from the competition of the resonant and non-resonant paths. One obtains the amplitude ratio $W \equiv \tilde{c}_S/\tilde{c}_D$ and the phase-shift difference δ from the anisotropy parameters using the relations [27, 28]

$$\beta_2 = \frac{10}{W^2 + 1} \left[\frac{1}{7} - \frac{W}{\sqrt{5}} \cos \delta \right], \quad \beta_4 = \frac{18}{7(W^2 + 1)}. \quad (17)$$

It should be noted that the values of β_2 , β_4 , W , and δ obtained as above are integrated over photoelectron energy. We calculate, on the other hand, energy-resolved values from c_S and c_D obtained by directly projecting the S and D partial waves onto the Coulomb wave functions.

B. Helium atom

To describe the photoionization of He atom we use direct numerical solution of the full-dimensional two-electron TDSE in the length gauge [57],

$$i \frac{\partial \Phi(\mathbf{r}_1, \mathbf{r}_2, t)}{\partial t} = [H_e + (z_1 + z_2)(E_X(t) + E_{IR}(t - \tau))] \Phi(\mathbf{r}_1, \mathbf{r}_2, t), \quad (18)$$

with the atomic Hamiltonian,

$$H_e = -\frac{1}{2} \nabla_1^2 - \frac{1}{2} \nabla_2^2 - \frac{2}{r_1} - \frac{2}{r_2} + \frac{1}{|\mathbf{r}_1 - \mathbf{r}_2|}. \quad (19)$$

We solve Eq. (18) numerically using the time-dependent close-coupling method [57–61]. Similarly to the case of a hydrogen atom, sufficiently long after the pulse has ended, the ionized wave packet moving outward in time is spatially well separated and clearly distinguishable from the non-ionized part remaining around the origin. We calculate photoelectron-energy-integrated β_2 and β_4 by integrating the ionized part of $|\Phi(\mathbf{r}_1, \mathbf{r}_2)|^2$ over $r_1, r_2, \theta_2, \phi_1, \phi_2$, from which one obtains W and δ by solving Eqs. (17). We use the values of δ_{sc} from [56] to calculate $\delta_{ex} = \delta - \delta_{sc}$.

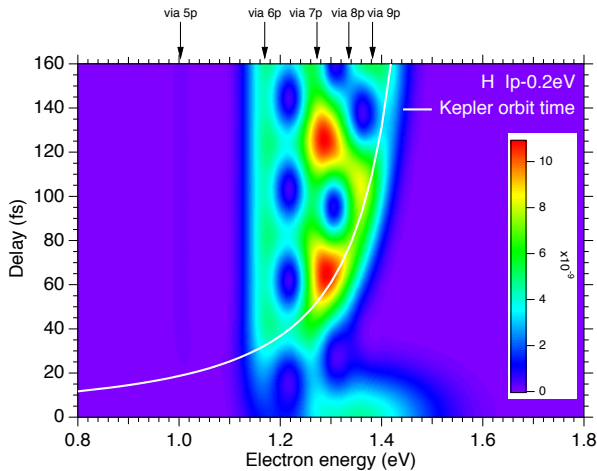


FIG. 1: (color online) False-color representation of photoelectron energy spectra as a function of time delay for the case of H atom. Above the top axis, the energy positions corresponding to a single IR photon ionization from each of $5p$ - $9p$ levels are indicated with vertical arrows. White solid line: the Kepler orbit time corresponding to $E_{\text{kin}} - \hbar\omega_L$ (see text).

C. Neon and argon atoms

For multi-electron atoms, like Ne and Ar, direct numerical solution of Eq. (13) is impossible. In many cases it is sufficient to solve the TDSE for one electron only (single active electron approximation) ignoring electron-electron correlations and influence of external electromagnetic fields on the other electrons [62–64]. In the present study we use this approach for two-color photoionization of Ne and Ar. In contrast to H and He cases, in Ne and Ar atoms the outermost “active” electron has p -symmetry and therefore it can be initially in p_σ ($m = 0$) and p_π ($m = 1$) states. Due to axial symmetry of the problem, ionization of states with σ ($m = 0$) and π ($m = 1$) symmetry can be considered independently and then the obtained cross sections should be summed incoherently.

Since the magnitude of the considered EUV field is comparatively low and its frequency is high, we use the first order perturbation treatment and the rotating wave approximation (RWA) for the description of the EUV-pulse interaction with the atomic p -electron. Thus, we present the active electron wave function as the following sum,

$$\Phi_{pm}(\mathbf{r}, t) = \exp(-i\epsilon_p t)\phi_{pm}^{(0)}(\mathbf{r}) + \phi_{pm}(\mathbf{r}, t). \quad (20)$$

Here ϵ_p is the binding energy of the electron in the initial state, $\phi_{pm}(\mathbf{r}, t)$ describes a perturbation of the active electron wave function due to interaction with the EUV field, and $\phi_{pm}^{(0)}(\mathbf{r})$ is the wave function of the active electron in the initial state. Within the RWA, the TDSE for an active p -electron can be

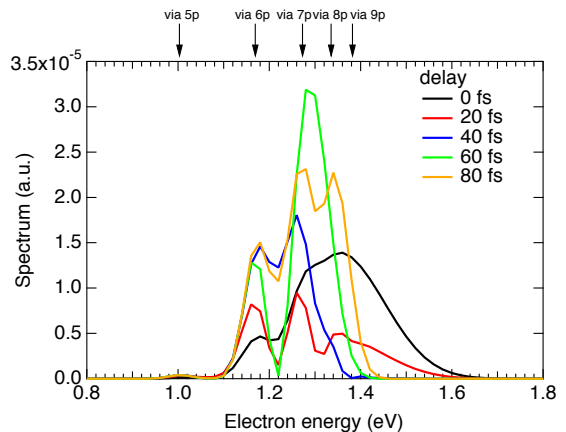


FIG. 2: (color online) Photoelectron energy spectra for H atom for several values of time delay indicated in the legend. Above the top axis, the energy positions corresponding to a single IR photon ionization from each of $5p$ - $9p$ levels are indicated with vertical arrows.

written as,

$$i\frac{\partial\phi_{pm}(\mathbf{r}, t)}{\partial t} = \left[-\frac{1}{2}\nabla^2 + U(r) - zE_{IR}(t - \tau) \right] \phi_{pm}(\mathbf{r}, t) - \frac{1}{2}z\bar{E}_X(t) \exp(-i(\epsilon_p + \omega_X)t)\phi_{pm}^{(0)}(\mathbf{r}), \quad (21)$$

where ω_X and $\bar{E}_X(t)$ denote the carrier frequency and the envelope of the EUV pulse, respectively. The interaction of the active electron with the ion core is taken into account by the effective single-electron potential $U(r)$. In the present study for the atoms Ne and Ar we have used the Herman-Skillman potential obtained within the Hartree-Slater approximation [65]. To solve Eq. (21) we used a method based on the expansion of the wave packet $\phi_{pm}(\mathbf{r}, t)$ in partial waves. The method is described in details in Refs. [63, 64]. The calculated double differential cross section was further used for calculating the asymmetry parameters β_n as functions of photoelectron energy.

IV. RESULTS AND DISCUSSION

A. Show-case of hydrogen atom two-photon near-threshold ionization

In this subsection we discuss in detail TPSI of a hydrogen atom as a show case demonstrating all peculiarities of the process of the two-color near-threshold ionization. The parameters of the pulses are given in Sec. III. In addition, the peak EUV intensity is set to 10^6 W/cm² (the process under consideration is basically linear in EUV intensity). The time delay between the pulse peaks is varied from 0 (complete overlap)

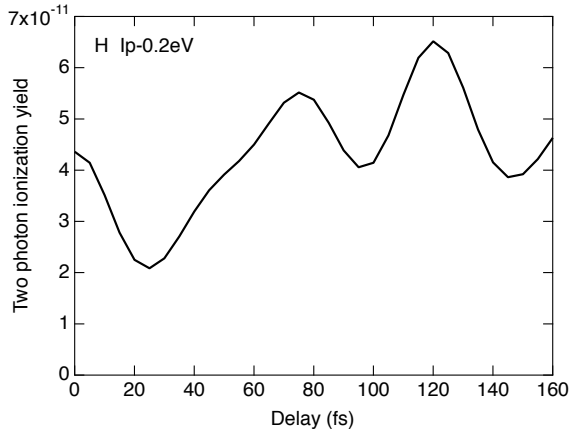


FIG. 3: Photoelectron yield from H atom as a function of time delay

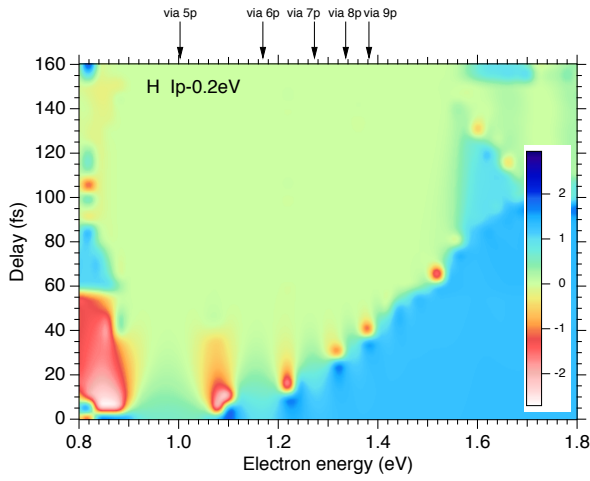


FIG. 4: (color online) False-color representation of the extra phase shift difference δ_{ex} as a function of time delay and photoelectron energy for H atom. Above the top axis, the energy positions corresponding to a single IR photon ionization from each of $5p$ - $9p$ levels are indicated with vertical arrows.

to 160 fs where the IR pulse is completely separated from the preceding EUV pulse.

Figure 1 illustrates how the photoelectron energy spectrum varies with the delay between the pulses in false-color representation. Figure 2 plots the spectra for several values of delay from 0 to 80 fs. The results are shown for the EUV photon energy of 13.405 eV, which is 0.2 eV below threshold ($E_{ex} = -0.2$ eV). In these figures, the kinetic energy positions $E_{kin} = \omega_L - \frac{1}{2n^2}$ ($n = 5, \dots, 9$) corresponding to a single IR photon ionization from each of $5p$ - $9p$ levels are indicated with vertical arrows. At $\tau = 0$ where the two pulses overlap each other, resonant peaks are embedded in a broad spectrum due to non-resonant processes, centered at $E_{kin} = \hbar\omega_X + \hbar\omega_L - I_p(\text{H}) = \hbar\omega_L + E_{ex} = 1.35$ eV. With increasing delay, the spectrum is dominated by resonant peaks, and the components between the peaks exhibit clear interference pattern, related with the evolution of the Rydberg

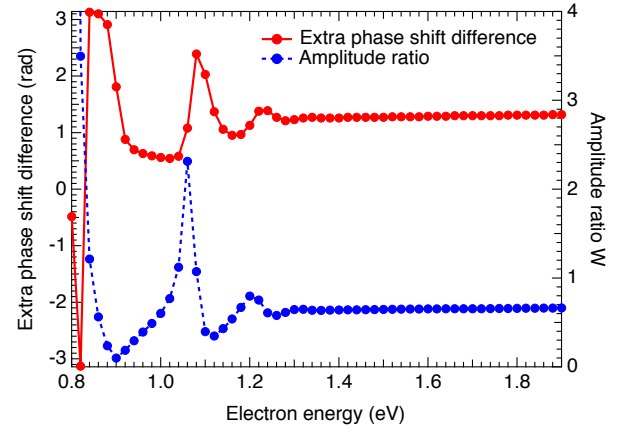


FIG. 5: (color online) Extra phase shift difference δ_{ex} (left axis) and amplitude ratio W (right axis) as a function of photoelectron energy for $\tau = 0$ for H atom.

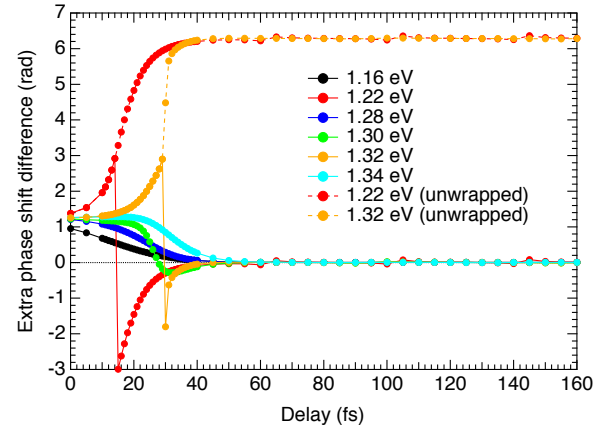


FIG. 6: (color online) Extra phase shift difference δ_{ex} as a function of time delay for H atom for several photoelectron energies indicated in the legend. Solid: wrapped within the range $-\pi \leq \delta_{ex} \leq \pi$, dashed (for 1.22 and 1.32 eV): unwrapped with a modulus of 2π .

wave packet created by the EUV pulse. The white solid line in Fig. 1 plots the nominal Kepler orbit time,

$$\tau_n = 2\pi n^3, \quad (22)$$

corresponding to a Rydberg state with the principal quantum number n from which the photoelectron energy is achieved through an IR photon absorption, i.e., $E_{kin} = \omega_L - \frac{1}{2n^2}$. One can see that this line indeed coincides with the first interference maximum. Due to this Rydberg wave packet dynamics, the two-photon ionization yield integrated over the photoelectron energy E_{kin} oscillates with the delay [Fig. 3].

We show in Fig. 4 the extra phase shift difference δ_{ex} as a function of time delay and photoelectron energy in false-color representation. While δ_{ex} is finite at zero delay, it varies with increasing delay and vanishes at large delay within the energy range ($1.0 \text{ eV} \lesssim E_{kin} \lesssim 1.5 \text{ eV}$) of photoelectrons, as predicted in Sec. II. Figure 5 plots the dependence of δ_{ex} and W on photoelectron energy. In the low-energy part, they

oscillate, reflecting changing relative contribution of resonant and non-resonant paths, whereas they are nearly constant in the high-energy part ($\gtrsim 1.3$ eV) for which $E_{\text{kin}} - \hbar\omega_L$ lies in the Rydberg manifold whose level spacing is much smaller than the spectral width.

One can see from Fig. 4 that the variation of δ_{ex} with increasing delay is not necessarily monotonic. To take a closer look at this, we plot the delay-dependence of δ_{ex} for several photoelectron energies in Fig. 6. For 1.16, 1.28, and 1.34 eV with a single dominant intermediate state ($6p$, $7p$, and $8p$, respectively), δ_{ex} decreases monotonically towards zero. On the other hand, for 1.30 eV where paths from $7p$ and $8p$ interfere with each other, δ_{ex} first decreases to a negative value before increasing again to zero. The extra phase shift difference δ_{ex} exhibits even more peculiar behavior at 1.22 and 1.32 eV, where the photoelectron yield strongly oscillates with delay (see Fig. 1); plotted within the range $[-\pi, \pi]$ (solid lines), δ_{ex} jumps at a certain delay. Actually, if unwrapped with a modulus of 2π (dashed lines), it increases monotonically to 2π . Small kinks around $\tau = 60, 100, 140$ fs for $E_{\text{kin}} = 1.22$ eV are due to slight numerical instability stemming from vanishing c_S and/or c_D , whose phases become undetermined.

Finally, we show the delay-dependence of photoelectron-energy integrated asymmetry parameters β_2 and β_4 as well as the amplitude ratio W and relative phase δ in Fig. 7. As expected, all of them vary with delay and tend to constant values. In particular, δ asymptotically tends to the scattering phase shift difference ($\delta_{sc} = 2.274$), or equivalently, $\delta_{ex} (= \delta - \delta_{sc})$ tends to zero.

B. Two-photon ionization of noble gas atoms

1. He atom

The case of He is of special interest since several measurements of the PADs from two-color TPSI of He have been reported [36, 38–42]. Moreover, in Refs. [36, 38, 39] a dependence of the PADs on the time delay between the pulses were investigated. In Ref. [36], however, the time-delay dependence was studied on the attosecond scale and is connected with the relative phase of the EUV and IR pulses which is outside the scope of our investigation. On the other hand, in Refs. [38, 39] two-color TPSI of He atom in both the below- and above-threshold cases was studied and no time-delay dependence of the PADs on the femtosecond scale was detected within experimental errors. At first sight this result contradicts to our main thesis that the PADs should depend on the delay between EUV and IR pulses. To clarify this situation we performed accurate two-electron TDSE calculations for the EUV photon energy which is 0.2 eV below the ionization threshold. Due to limitation of the computation time we made calculations for an IR pulse duration of 10 fs with a peak EUV intensity of 10^{10} W/cm² and all the other parameters indicated in Sec. III. The results of calculations are shown in Fig. 8 as solid curves. One sees that indeed the asymmetry parameters β_2 and β_4 as well as the amplitude ratio W and the relative phase δ between the S and D partial waves are practically

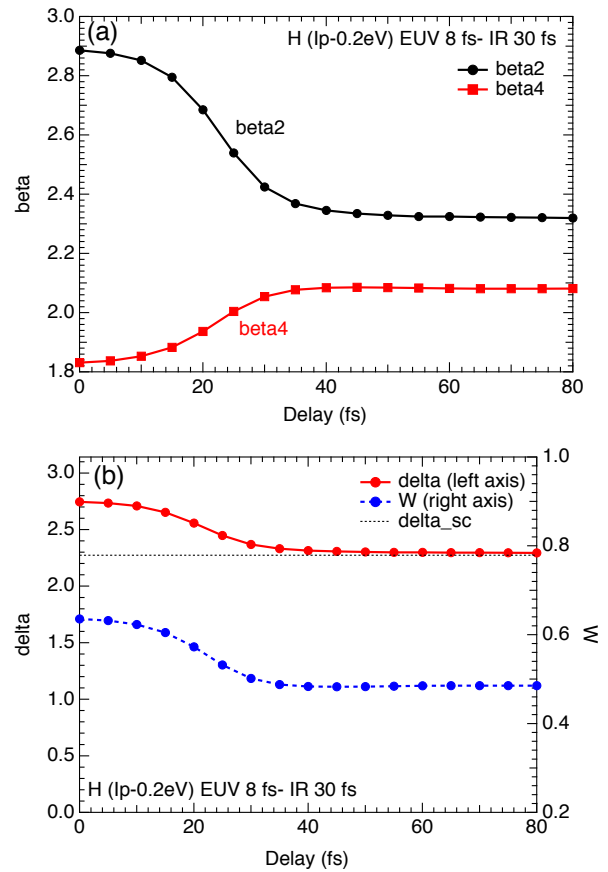


FIG. 7: (color online) Time-delay dependence of the energy-integrated (a) asymmetry parameters β_2 and β_4 , and (b) the relative phase δ (left axis) and amplitude ratio W (right axis) in TPSI of H atoms. Thin dashed curve: the scattering phase shift difference $\delta_{sc} = 2.274$ (left axis).

independent of the time-delay, in agreement with the experimental reports [38, 39]. The value of δ is found to be close to the scattering phase shift difference $\delta_{sc} = 2.696$ [56].

We have also made calculations for the same parameters within the single-active electron approximation using the same TDSE code as for Ne and Ar. In this case the effective single-electron potential was chosen as a screened Coulomb potential with a polarization term:

$$U(r) = -\frac{2}{r} - \frac{1}{r} (e^{-4r} - 1) - 2e^{-4r} - \frac{9}{32(r^2 + 1.2)^2}. \quad (23)$$

The results shown in Fig. 8 (dashed curves) are in good agreement with a more elaborate calculations with the two-electron TDSE. Moreover, we made single-electron calculations for a longer IR pulse of 30 fs and have found that the beta parameters for He are practically independent of the IR pulse duration. Thus we have proved that in He case, in agreement with the experiment [38, 39], the PADs are practically independent of the time delay between the pulses. The He atom indeed represents a special case in which the PAD barely varies with delay, accidentally, for the particular combination of photon energies used.

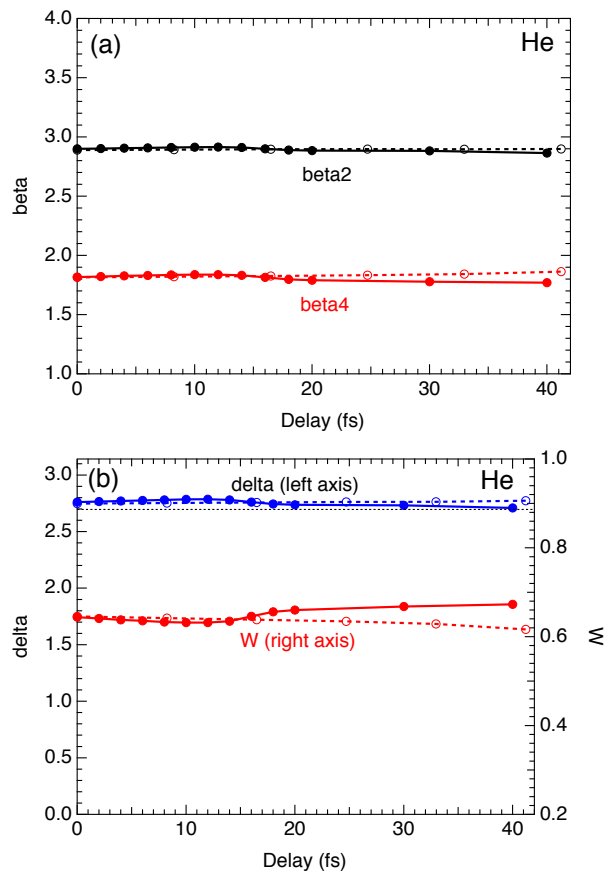


FIG. 8: (color online) Time-delay dependence of the energy-integrated (a) asymmetry parameters β_2 and β_4 , and (b) the relative phase δ (left axis) and amplitude ratio W (right axis) in TPSI of He atoms. Thick solid curves: two-electron TDSE simulations. Thin dashed curve in (b): the scattering phase shift difference $\delta_{sc} = 2.696$ (left axis) [56].

In order to investigate this interesting case further we have calculated the electron spectra for different time delays using single active electron approximation. The spectra integrated over emission angle are shown in Fig. 10. They are marked by the numbers which indicate different relative position of the maxima of the EUV and IR pulses as shown in Fig. 9. Curve 1 corresponds to a complete overlap of the pulses where their maxima coincide. Curve 9 corresponds to another extreme case where the pulses are separated, the EUV pulse acting first to the atom.

One can see from Fig. 10 that the photoelectron spectrum strongly varies with the time-delay, in striking contrast to β parameters. Its shape, position of the main maximum and its width depend on the delay, reflecting the interplay between resonant and non-resonant mechanism of ionization. The variations of the spectra are qualitatively similar to the case of hydrogen atom (Fig. 2). When the delay is zero (line 1), both resonant and non-resonant transitions contribute, (see Sec. II), the spectrum is broad with the maximum at $\hbar\omega_L + E_{ex} = 1.35$ eV. Its width is mainly determined by that

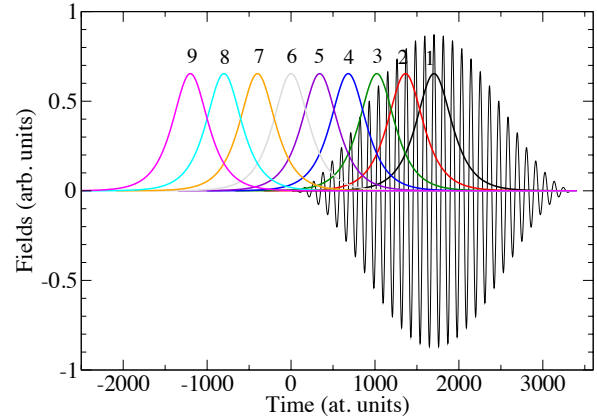


FIG. 9: (color online) The electric field of the 30 fs IR pulse (thin black curve) and the envelopes of the electric field of the EUV pulses (thick colored curves) in arbitrary units for different time delays. Numbers indicate the following delays between EUV and IR pulses: 1 - 0 fs (complete overlap); 2 - 8.2 fs; 3 - 16.5 fs; 4 - 24.7 fs; 5 - 33 fs; 6 - 41.2 fs; 7 - 50.9 fs; 8 - 60.6 fs; 9 - 70.2 fs (fully separated pulses)

(0.23 eV) of the shorter EUV pulse (8 fs). In the other extreme case of non-overlapping pulses (curve 9) particular Rydberg states (presumably mainly $1s7p$ and $1s8p$ states [66]) are resonantly excited by the EUV pulse, which are then ionized by the IR pulse. The main maximum is red shifted since the lower Rydberg states are predominantly populated. The width of the peak is smaller since it is now determined mainly by that (0.06 eV) of the longer IR pulse (30 fs). Small maximum on the left side of the main peak corresponds to ionization through excitation of the $1s6p$ Rydberg state. In the intermediate cases of partial overlap of the pulses one observes gradual transition to the pure resonant case with interference of ionization paths via $1s6p$, $1s7p$, and $1s8p$ states.

The energy-resolved angular distributions calculated at different parts of the spectrum are practically the same and do not change in spite of the variation of the spectrum, which leads to a practical independence of the β parameters from the pulse overlap.

2. Ne and Ar atoms

In this subsection we present the simulation results for Ne and Ar atoms. In both cases the EUV photon energy was chosen to be 0.2 eV below the corresponding ionization thresholds. In such a case, a group of Rydberg states is excited by the EUV pulse, which is then ionized by an IR photon. For chosen energy of IR photon (1.55 eV) one can expect a group of photoelectrons with the energy about 1.35 eV. In Fig. 11 we show the angle-integrated spectra of photoelectrons from Ne calculated for different time delays between EUV and IR pulses from complete overlap of the pulses (curve 1) to fully separated pulses (curve 9). The numbers on the curves corre-

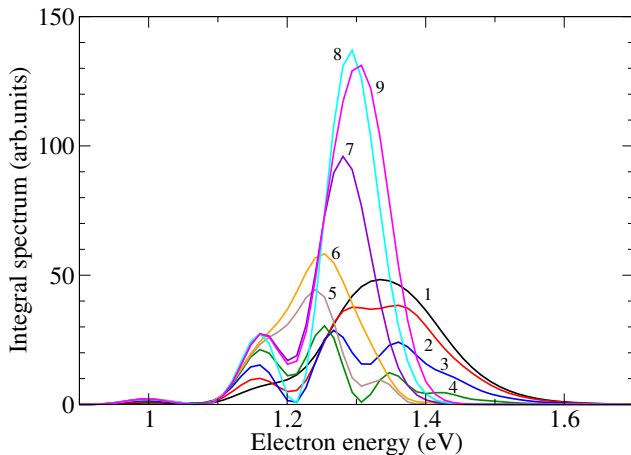


FIG. 10: (color online) The angle-integrated electron spectrum for TPSI of He for varies time delays shown in Fig. 9. The numbers at the curves correspond to the numbers which mark different positions of the EUV peak in Fig. 9.

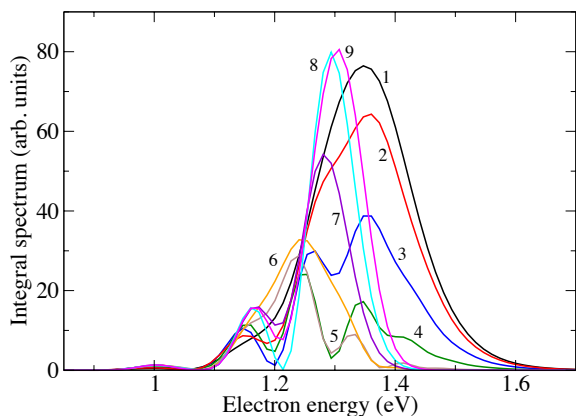


FIG. 11: (color online) The same as in Fig. 10 but for $2p$ ionization of Ne atoms.

spond to the delays displayed in Fig. 9. As in the case of H and He, the shape of the spectrum and its width strongly depends on the delay. It is mainly determined by the interplay of the resonant and non-resonant contributions to the ionization as discussed above.

For all delays we have also calculated the energy dependence of the asymmetry parameters β_2 , β_4 and β_6 , where β_6 is the next coefficient in the expansion of the PAD in terms of Legendre polynomials. In all cases the latter parameter is at least two orders of magnitude smaller than the first two. This confirms that at the chosen IR intensity of 10^{10} W/cm² only one IR photon is absorbed. Together with the EUV excitation it gives two-photon ionization with angular distribution of photoelectrons described by Eq. (12). As an example in Fig. 12 we show the photoelectron spectrum from Ne and β parameters as functions of photoelectron energy for the case

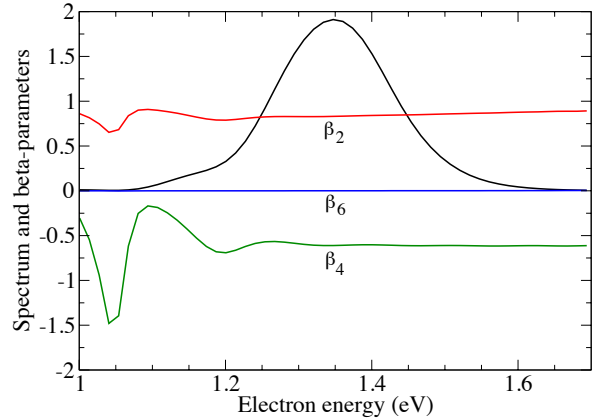


FIG. 12: (color online) The electron spectra (in arbitrary units) and evolution of the asymmetry parameters across the resonance for zero time delay between EUV and IR pulses calculated for Ne atom.

of complete overlap of the EUV and IR pulses (case 1 in Fig. 9). Interestingly, the parameters β_2 and β_4 are practically constant in the region of maximum, changing their value only when the cross section is small, which is consistent with the hydrogen case (see Fig. 5). Similar behavior is observed for all other delays.

In Fig. 13 we show the calculated β_2 and β_4 parameters for the angular distribution integrated over the peak, as it is usually measured in real experiments. The parameters are shown as functions of time delay. One sees that both parameters are changing considerably with the delay. The β_4 even changes its sign. This behavior was predicted theoretically and confirmed by experiment in our recent publication [43].

Similar calculations have been done for Ar. The calculated photoelectron spectra integrated over the emission angle are presented in Fig. 14 for several delays between pulses. Qualitatively the spectra and their variation with the time-delay are similar to the cases of H (Fig. 2), He (Fig. 10) and Ne (Fig. 11). This is natural since the properties of the Rydberg states close to the threshold depend only weakly on the properties of the core.

Figure 15 shows the values of β_2 and β_4 for the case of Ar, calculated for various time-delays. Similar to the Ne case the asymmetry parameters notably depend on the delay. Interestingly, in the Ar case the β_4 parameter does not change its sign unlike in the case of Ne. This difference is possibly explained by different s and d excitation by the EUV pulse in Ne and Ar [67].

According to our calculations the variation of the β_2 and β_4 parameters with the time delay is much more pronounced for Ne and Ar than for H and He atoms. Presumably, this is related to the fact that in Ne and Ar p -electron is ionized. In this case the PAD in two-photon ionization is defined mainly by the contribution of P and F partial wave packets which can give more space for beta variations. In particular, the β_4 parameter in s -ionization depends only on the ratio W of S and

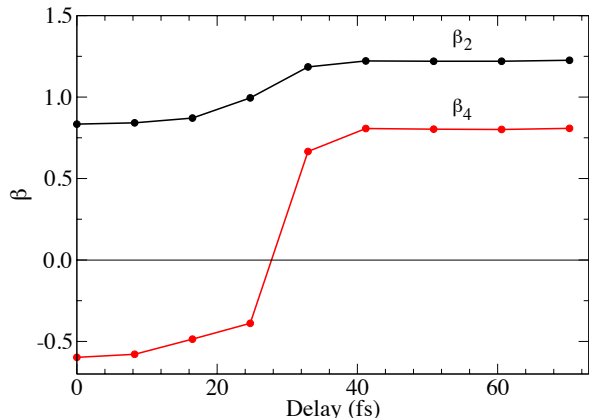


FIG. 13: (color online) The calculated dependence of asymmetry parameters β_2 and β_4 on delay between EUV and IR pulses for the case of Ne ionization at EUV photon energy -0.2 eV below threshold. The parameters are shown for the angular distribution integrated over the peak. The points are connected by straight lines to guide the eye.

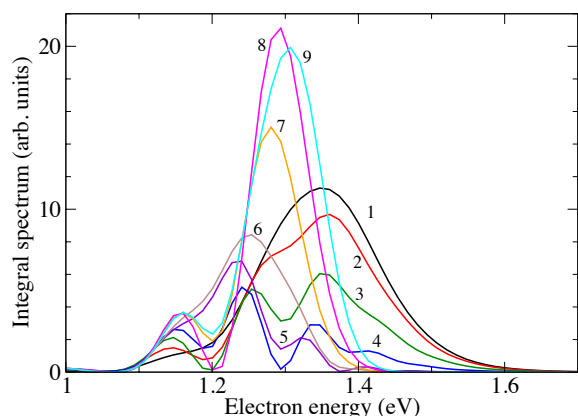


FIG. 14: (color online) Photoelectron spectra integrated over emission angle for different time-delays indicated in Fig. 9, calculated for 3p ionization of Ar.

D amplitudes (see Eqs. (17)), while in p -ionization it depends on both the amplitude ratio and relative phase of P and F partial waves, which may be more sensitive to the contribution of resonant and non-resonant pathways.

V. CONCLUSIONS

We have theoretically investigated the PADs for two-color (EUV+IR) TPSI of H, He, Ne, and Ar atoms with EUV excitation slightly below the ionization threshold. The PADs for EUV+IR TPSI have recently been experimentally mea-

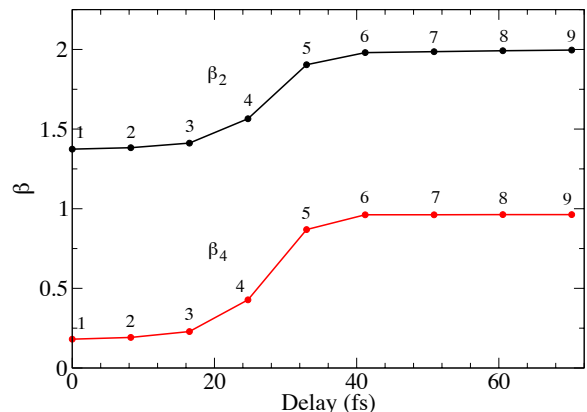


FIG. 15: (color online) Photoelectron angular distribution parameters β_2 and β_4 for photoionization of Ar atom as functions of time-delay. Numbers indicate the particular delays shown in Fig. 9. The points are connected by straight lines to guide the eye.

sured with modern EUV FEL and high-harmonic sources. We have shown that the photoelectron energy spectra as well as anisotropy parameters β_2 and β_4 strongly depend on the time delay between the EUV and IR pulses, except for β values for the case of He. This dependence is associated with the contributions of the resonant and nonresonant pathways of ionization, changing with the pulse delay, which implies that investigations of the time-delay dependence of the PADs in TPSI make it possible to study the fundamental problem of the interplay of resonant and nonresonant processes in photoionization. Our results indicate that the variation of PADs with the time delay is more pronounced for ionization of p -shell electrons (Ne and Ar) than for s -shell electrons (H and He). Surprisingly, the anisotropy parameters barely changes with delay for the case of He for the present combination of photon energies. This explains why the delay dependence was not detected in [38].

Acknowledgments

KLI gratefully acknowledges support by KAKENHI (Grants No. 23656043, No. 25286064, and No. 26600111), the Photon Frontier Network program of MEXT (Japan), the Center of Innovation Program from JST (Japan), and the Cooperative Research Program of “Network Joint Research Center for Materials and Devices” (Japan). KLI also thanks Mr. Y. Futakuchi and Ms. S. Watanabe for their help in Fig. 6 and reference preparation, respectively. NMK acknowledges financial support from the programme ‘Physics with Accelerators and Reactors in West Europe’ of the Russian Ministry of Education and Science. He also acknowledges hospitality and financial support from XFEL (Hamburg). KU is grateful to the Ministry of Education, Culture, Sports, Science, and Technology of Japan for supports via X-ray Free Electron Laser

Utilization Research Project, the X-ray Free Electron Laser Priority Strategy Program, and Management Expenses Grants

for National Universities Corporations.

-
- [1] *VUV and Soft X-ray Photoionization*, edited by U. Becker and D. A. Shirley (Plenum Press, New York, 1996).
- [2] Y. Gontier and M. Trahin, *Phys. Rev. A* **4**, 1896 (1971).
- [3] B. L. Beers and L. Armstrong, *Phys. Rev. A* **12**, 2447 (1975).
- [4] M. Crance and S. Feneuille, *Phys. Rev. A* **16**, 1587 (1977).
- [5] D.L. Andrews, *J. Phys. B* **10**, L659 (1977).
- [6] W. A. McClean and S. Swain, *J. Phys. B* **11**, 1717 (1978).
- [7] W. A. McClean and S. Swain, *J. Phys. B* **12**, 2291 (1979).
- [8] R. I. Jackson, D. P. O'Brien, and S. Swain, *J. Phys. B* **15**, 3385 (1982).
- [9] S. N. Dixit and P. Lambropoulos, *Phys. Rev. A* **27**, 861 (1983).
- [10] D. Proulx and R. Shakeshaft, *J. Phys. B* **26**, L7 (1993).
- [11] A. Saenz and P. Lambropoulos, *J. Phys. B* **32**, 5629 (1999).
- [12] L. A. A. Nikolopoulos and P. Lambropoulos, *J. Phys. B* **34**, 545 (2001).
- [13] K. Ishikawa and K. Midorikawa, *Phys. Rev. A* **65**, 043405 (2002).
- [14] H. W. van der Hart and P. Bingham, *J. Phys. B* **38**, 207 (2005).
- [15] S. Selstø, A. Palacios, J. Fernandez, and F. Martin, *Phys. Rev. A* **75**, 033419 (2007).
- [16] H. R. Varma, M. F. Ciappina, N. Rohringer, and R. Santra, *Phys. Rev. A* **80**, 053424 (2009).
- [17] K. L. Ishikawa, Y. Kawazura, and K. Ueda, *J. Modern Optics* **57**, 999 (2010).
- [18] Y. Koboyashi, T. Sekikawa, Y. Nabekawa, and S. Watanabe, *Opt. Lett.* **23**, 64 (1998).
- [19] T. Sekikawa, A. Kosuge, T. Kanai, and S. Watanabe, *Nature* **432**, 605 (2004).
- [20] N. Miyamoto, M. Kamei, D. Yoshitomi, T. Kanai, T. Sekikawa, T. Nakajima, and S. Watanabe, *Phys. Rev. Lett.* **93**, 083903 (2004).
- [21] H. Hasegawa, E. J. Takahashi, Y. Nabekawa, K. L. Ishikawa, and K. Midorikawa, *Phys. Rev. A* **71**, 023407 (2005).
- [22] A. A. Sorokin, M. Wellhöfer, S. V. Bobashev, K. Tiedtke, and M. Richter, *Phys. Rev. A* **75**, 051402(R) (2007).
- [23] V. Richardson, J. T. Costello, D. Cubaynes, S. Düsterer, J. Feldhaus, H. W. van der Hart, P. Juranić, W. B. Li, M. Meyer, M. Richter, A. A. Sorokin, and K. Tiedtke, *Phys. Rev. Lett.* **105**, 013001 (2010).
- [24] R. Moshhammer, T. Pfeifer, A. Rudenko, Y. H. Jiang, L. Foucar, M. Kurka, K. U. Kühnel, C. D. Schröter, J. Ullrich, O. Herrwerth, M. F. Kling, X. J. Liu, K. Motomura, H. Fukuzawa, A. Yamada, K. Ueda, K. L. Ishikawa, K. Nagaya, H. Iwayama, A. Sugishima, Y. Mizoguchi, S. Yase, M. Yao, N. Saito, A. Belkacem, M. Nagasono, A. Higashiya, M. Yabashi, T. Ishikawa, H. Ohashi, H. Kimura, and T. Togashi, *Opt. Express* **19**, 21698 (2011).
- [25] T. Sato, A. Iwasaki, K. Ishibashi, T. Okino, K. Yamanouchi, J. Adachi, A. Yagishita, H. Yazawa, F. Kannari, M. Aoyama, K. Yamakawa, K. Midorikawa, H. Nakano, M. Yabashi, M. Nagasono, A. Higashiya, and T. Ishikawa, *J. Phys. B* **44**, 161001 (2011).
- [26] R. Ma, K. Motomura, K. L. Ishikawa, S. Mondal, H. Fukuzawa, A. Yamada, K. Ueda, K. Nagaya, S. Yase, Y. Mizoguchi, M. Yao, A. Rouze, A. Hundermark, M. J. J. Vrakking, P. Johnsson, M. Nagasono, K. Tono, T. Togashi, Y. Senba, H. Ohashi, M. Yabashi, and T. Ishikawa, *J. Phys. B* **46**, 164018 (2013).
- [27] K. L. Ishikawa and K. Ueda, *Phys. Rev. Lett.* **108**, 033003 (2012).
- [28] K. L. Ishikawa and K. Ueda, *Applied Sciences* **3**, 189 (2013).
- [29] T. E. Glover, R. W. Schoenlein, A. H. Chin, and C. V. Shank, *Phys. Rev. Lett.* **76**, 2468 (1996).
- [30] E. S. Toma, H. G. Müller, P. M. Paul, P. Breger, M. Cheret, P. Agostini, C. Le Blanc, G. Mullot, and G. Cheriaux, *Phys. Rev. A* **62**, 061801(R) (2000).
- [31] M. Meyer, D. Cubaynes, P. O'Keeffe, H. Luna, P. Yeates, E. T. Kennedy, J. T. Costello, P. Orr, R. Taïeb, A. Maquet, S. Düsterer, P. Radcliffe, H. Redlin, A. Azima, E. Plönjes, and J. Feldhaus, *Phys. Rev. A* **74**, 011401 (2006).
- [32] M. Meyer, D. Cubaynes, D. Glijer, J. Dardis, P. Hayden, P. Hough, V. Richardson, E. T. Kennedy, J. T. Costello, P. Radcliffe, S. Düsterer, A. Azima, W. B. Li, H. Redlin, J. Feldhaus, R. Taïeb, A. Maquet, A. N. Grum-Grzhimailo, E. V. Gryzlova, and S. I. Strakhova, *Phys. Rev. Lett.* **101**, 193002 (2008).
- [33] M. Fushitani, Y. Hikosaka, A. Matsuda, T. Endo, E. Shigemasa, M. Nagasono, T. Sato, T. Togashi, M. Yabashi, T. Ishikawa, and A. Hishikawa, *Phys. Rev. A* **88**, 063422 (2013).
- [34] M. Meyer, J. T. Costello, S. Düsterer, W. B. Li, and P. Radcliffe, *J. Phys. B* **43**, 194006 (2010).
- [35] O. Guyétand, M. Gisselbrecht, A. Huetz, P. Agostini, R. Taïeb, V. Vénier, A. Maquet, L. Antonucci, O. Boyko, C. Valentin, and D. Douillet, *J. Phys. B* **38**, L357 (2005).
- [36] O. Guyétand, M. Gisselbrecht, A. Huetz, P. Agostini, R. Taïeb, A. Maquet, B. Carré, P. Breger, O. Gobert, D. Garzella, J-F Hergott, O. Tcherbakoff, H. Merdji, M. Bougeard, H. Rottke, M. Böttcher, Z. Ansari, and P. Antoine, *J. Phys. B* **41**, 051002 (2008).
- [37] L. H. Haber, B. Doughty, and S. R. Leone, *J. Phys. Chem. A* **113**, 13152 (2009).
- [38] L. H. Haber, B. Doughty, and S. R. Leone, *Phys. Rev. A* **79**, 031401(R) (2009).
- [39] L. H. Haber, B. Doughty, and S. R. Leone, *Molecular Physics* **108**, 1241 (2010).
- [40] L. H. Haber, B. Doughty, and S. R. Leone, *Phys. Rev. A* **84**, 013416 (2011).
- [41] P. O'Keeffe, A. Mihelic, P. Bolognesi, M. Zitnik, A. Moise, R. Richter, and L. Avaldi, *N. J. Phys.* **15**, 013023 (2013).
- [42] S. Mondal, H. Fukuzawa, K. Motomura, T. Tachibana, K. Nagaya, T. Sakai, K. Matsunami, S. Yase, M. Yao, S. Wada, H. Hayashita, N. Saito, C. Callegari, K. C. Prince, P. O'Keeffe, P. Bolognesi, L. Avaldi, C. Miron, M. Nagasono, T. Togashi, M. Yabashi, K. L. Ishikawa, I. P. Sazhina, A. K. Kazansky, N. M. Kabachnik, and K. Ueda, *J. Phys. B* **46**, 205601 (2013).
- [43] S. Mondal, H. Fukuzawa, K. Motomura, T. Tachibana, K. Nagaya, T. Sakai, K. Matsunami, S. Yase, M. Yao, S. Wada, H. Hayashita, N. Saito, C. Callegari, K. C. Prince, C. Miron, M. Nagasono, T. Togashi, M. Yabashi, K. L. Ishikawa, A. K. Kazansky, N. M. Kabachnik, and K. Ueda, *Phys. Rev. A* **89**, 013415 (2014).
- [44] N. Dudovich, B. Dayan, S. M. Gallagher Faeder, and Y. Silberberg, *Phys. Rev. Lett.* **86**, 47 (2001).
- [45] S. J. Smith and G. Leuchs, *Adv. At. Mol. Phys.* **24**, 157 (1988).
- [46] K. C. Kulander, K. J. Schafer, and J. L. Krause, in *Atoms in Intense Laser Fields*, edited by M. Gavrila (Academic, New York,

- 1992) pp. 247-300.
- [47] K. Ishikawa and K. Midorikawa, *Phys. Rev. A* **65**, 031403(R)(2002).
- [48] K. Ishikawa, *Phys. Rev. Lett.* **91**, 043002 (2003).
- [49] K. L. Ishikawa, *Phys. Rev. A* **74**, 023806 (2006).
- [50] K. L. Ishikawa, E. J. Takahashi, and K. Midorikawa, *Phys. Rev. A* **75**, 021801(R) (2007).
- [51] K. Schiessl, K. L. Ishikawa, E. Persson, and J. Burgdörfer, *Phys. Rev. Lett.* **99**, 253903 (2007).
- [52] K. L. Ishikawa, E. J. Takahashi, and K. Midorikawa, *Phys. Rev. A* **80**, 011807(R) (2009).
- [53] D. G. Arbó, K. L. Ishikawa, K. Schiessl, E. Persson, and J. Burgdörfer, *Phys. Rev. A* **81**, 021403(R) (2010).
- [54] D. H. Oza, *Phys. Rev. A* **33**, 824 (1986).
- [55] T. N. Chang and T. K. Fang, *Phys. Rev. A* **52**, 2638 (1995).
- [56] T. T. Gien, *J. Phys. B* **35**, 4475 (2002).
- [57] K. L. Ishikawa and K. Midorikawa, *Phys. Rev. A* **72**, 013407 (2005).
- [58] M. S. Pindzola and F. Robicheaux, *Phys. Rev. A* **57**, 318 (1998).
- [59] M. S. Pindzola and F. Robicheaux, *J. Phys. B* **31**, L823 (1998).
- [60] J. Colgan, M. S. Pindzola, and F. Robicheaux, *J. Phys. B* **34**, L457 (2001).
- [61] J. S. Parker, L. R. Moore, K. J. Meharg, D. Dundas, and K. T. Taylor, *J. Phys. B* **34**, L69 (2001).
- [62] A. K. Kazansky and N. M. Kabachnik, *J. Phys. B* **39**, 5173 (2006).
- [63] A. K. Kazansky and N. M. Kabachnik, *J. Phys. B* **40**, 2163 (2007).
- [64] A. K. Kazansky and N. M. Kabachnik, *J. Phys. B* **40**, 3413 (2007).
- [65] F. Herman and S. Skillman, *Atomic Structure Calculations* (Prentice-Hall, Englewood Cliffs NJ, 1963).
- [66] A. Kramida, Yu. Ralchenko, J. Reader and NIST ASD Team 2012, NIST Atomic Spectra Database (version 5.0) <http://physics.nist.gov/asd>.
- [67] D. J. Kennedy and S. T. Manson, *Phys. Rev. A* **5**, 227 (1972).